

TRAILING VORTICES GENERATED BY A RUSHTON TURBINE: ASSESSMENT OF RANS AND LARGE EDDY SIMULATIONS

A. Delafosse^a, J. Morchain^{a*}, P. Guiraud^a, A. Liné^a

^a *Laboratoire d'Ingénierie des Systèmes Biologiques et des Procédés, UMR CNRS 5504/INRA
792, Institut National des Sciences Appliquées, 135 avenue de Rangueil, 31400 Toulouse,
FRANCE; e-mail: Jerome.Morchain@insa-toulouse.fr*

Abstract. The discharge flow of a Rushton turbine is characterized by the formation of coherent vortex structures induced by the blade motion and called trailing vortices. The objective here is to assess the ability of CFD to represent the trailing vortices and their relationship with turbulence properties. To this end, two simulations have been realized: a RANS-based simulation and a LES simulation. The trajectory of the trailing vortices predicted by the simulations has been compared with previous works. This comparison shows that the RANS simulation does not predict properly the trailing vortices while the LES results are very close to the experimental ones. As a consequence, the turbulence properties spatially correlated to the trailing vortices are well predicted by LES but not by RANS simulation.

Key words: Trailing vortices, stirred tank, Rushton turbine, CFD, Large Eddy Simulation, RANS simulation

1. INTRODUCTION

In a stirred tank, the discharge flow of the impeller is characterized by the formation of coherent vortex structures induced by the blade motion and called trailing vortices. Because of the presence of a disk, two trailing vortices are generated behind a Rushton turbine: above and below the disk.

These trailing vortices have significant impact on mixing because they affect the impeller efficiency. Minimizing the vortex size improves the blending performance of an impeller. Moreover, in an aerated tank, gas bubbles introduced below the impeller interact with trailing vortices. The gas bubbles accumulate in the trailing vortices and this gas accumulation (or gas cavities) significantly alters flow around impeller region.

The aim of this study is to assess the ability of Computational Fluid Dynamics (CFD) to represent the trailing vortices generated by a Rushton turbine. Two simulations have been realized with the commercial computational code Fluent (v. 6.2.16): a simulation based on the Reynolds-Averaged Navier-Stokes equations with the k-epsilon model and a Large Eddy Simulation (LES) with the Smagorinski subgrid scale model.

In a previous paper [1], both RANS and LES simulations have been compared to experimental works in terms of mean velocity, kinetic energy and dissipation rate. Here, the trajectory of each trailing vortex has been determined and compared to various experimental and numerical works. A special emphasis is made on the relationship between trailing vortices

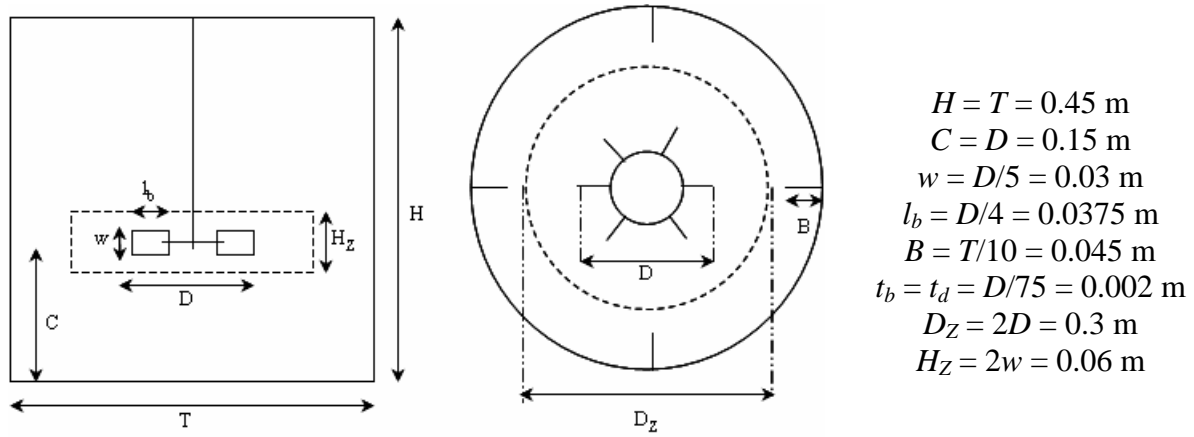


Fig. 1: Cross-section, plan view and dimensions of the stirred tank and the Rushton turbine.

and turbulence properties (turbulent kinetic energy and turbulence dissipation rate) in the impeller discharge.

2. COMPUTATIONAL TOOLS

2.1 Physical configuration

The geometry of the tank and the Rushton turbine used for the simulations is identical to that of the device used in a previous experimental (PIV) work [2,3,4]. The flat-bottom tank equipped with four flat baffles has a diameter $T = 0.45$ m and is filled up with water to a level $H = T = 0.45$ m, corresponding to a liquid volume of 0.07 m³. The Rushton turbine has a diameter $D = T/3 = 0.15$ m and is located at a clearance $C = D = 0.15$ m. All the dimensions used are presented on Fig. 1.

The geometry and the grid mesh were realized with the software Gambit. In order to use the sliding mesh technique, two fluid zones were defined: an inner rotating cylindrical volume centered on the impeller and an outer stationary zone, containing the rest of the tank and the baffles. The dimension of the rotating zone is $H_z = 60$ mm and $D_z = 300$ mm (see Fig. 1). For both RANS and LES simulations, the mesh used consists of approximately 250 000 and 750 000 hexahedrons for the rotating and the stationary zone respectively.

Although a RANS simulation does not need so fine a grid, the same grid has been used for both simulations, so that any influence of the grid size is avoided

2.2 Numerical details

The three dimensional simulations were performed using the commercial CFD code FLUENT 6.2.16. The working fluid is water ($\rho = 998.2$ kg.m⁻³ and $\mu = 10^{-3}$ kg.m⁻¹.s⁻¹). The impeller rotational speed is 150 rpm ($N = 2.5$ s⁻¹), resulting in a Reynolds number $Re = 56\ 250$.

With the use of sliding mesh, the flow resolution is unsteady. At each time step the position of the rotating zone relative to the stationary one is recomputed and the grid interface of the rotating zone slides along the interface of the stationary zone. The time step used for the simulations is $5.5556 \cdot 10^{-4}$ s, so that the angular displacement of the impeller zone per time step corresponds to 0.5° .

At the end of each time step, after a maximum of 20 iterations, the convergence criteria (residuals) reached a typical value of 10^{-4} for continuity, momentum (RANS and LES) and turbulence quantities (RANS only). The simulations are performed in double precision with the segregated implicit solver. The temporal discretization scheme is 2nd order for the two models of turbulence used. For RANS simulation, the spatial discretization scheme is 2nd

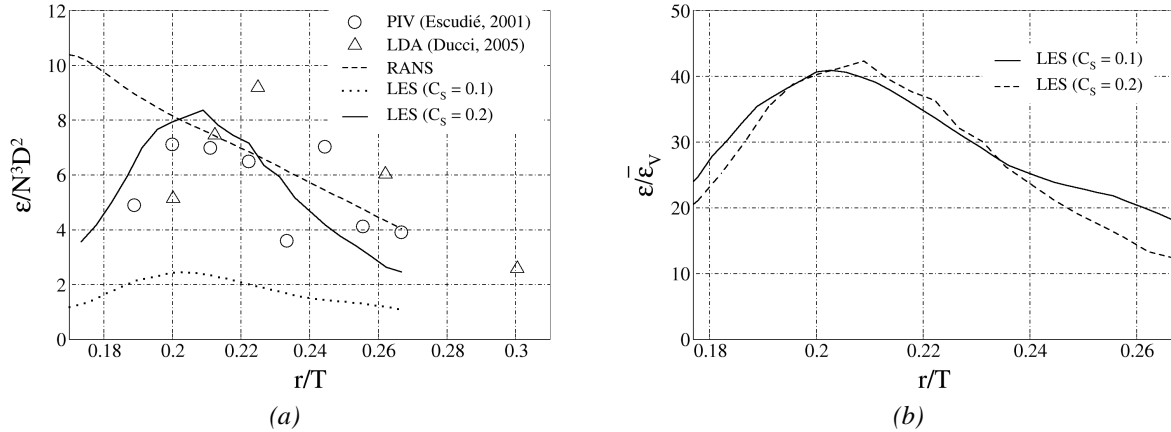


Fig. 2: Radial evolutions of (a) the local dissipation rate for numerical and experimental works and (b) the ratio local dissipation rate on overall dissipation rate for LES simulations with the 2 values of C_S used.

order for all quantities (continuity, momentum, turbulence). For LES, the spatial discretization is 2nd order for pressure and 3rd order for momentum.

2.3 Turbulence modelling

The closure model used for RANS simulation is the standard *k-epsilon* model implemented in FLUENT. The constants of the model are set to their default values.

For Large Eddy Simulation, the subgrid model used is the Smagorinski model based on the concept of eddy viscosity. The value of the Smagorinski constant is $C_S = 0.2$. We have shown in a previous paper [1] that the value of this constant has no influence on the velocity and kinetic energy fields. On the contrary, its influence on turbulence dissipation rate is quite strong. Between two simulations with $C_S = 0.1$ and $C_S = 0.2$ the local and overall dissipation rate increases by a factor 3.3. This trend is shown on Fig. 2 (a), where the radial evolution of the local dissipation rate is plotted for RANS and LES simulations with the 2 values of the constant used and for various experimental works [425]. On Fig. 2 (b) is plotted the ratio local dissipation rate on overall dissipation rate and it can be observed that, despite the influence of the constant C_S on the local and overall values of the turbulence dissipation rate, the ratio is quite constant. More detail can be found in [1].

3. RESULTS

3.1 Data processing

The locations of trailing vortices have been determined in a vertical plane located at the blade tip and between two baffles in the impeller discharge: $0.17 < r/T < 0.26$ and $0.27 < z/T < 0.4$.

For LES, a phase-averaged treatment was performed to extract the mean velocity, the periodic velocity fluctuations and the turbulent velocity fluctuations. 14400 acquisitions (velocities, velocity gradients...) have been realized, corresponding to 120 acquisitions for a fixed position of the blade relative to the acquisition plane and 20 complete rotations of the impeller.

For RANS simulation, the turbulent fluctuations are not resolved and the velocity field resolved at each time step corresponds to a phase-averaged field. Thus, 120 acquisitions, corresponding to the passage of two blades on the acquisition plane, are enough.

Several methods enable to determine the centre (or axis) of a trailing vortex. The most commonly used is based on phase-averaged axial velocity [6,7,8,9,10]. The mean vortex axis is defined as the location where the axial velocity component is zero. Another method is based on the vorticity magnitude [4,11,12,13,14]: the vortex axis is defined by the location of the maximum vorticity magnitude. A third method has been proposed by Jeong and Hussain

[15] and has been used in the work of Escudié *et al.* [4]. This method is based on the eigenvalues of the tensor $S^2 + \Omega^2$, where S and Ω are respectively the symmetric and the antisymmetric part of the velocity gradient tensor. It enables the location of the pressure minimum corresponding to the vortex core. A comparison between the vortex axis determined by the second and this last method has shown that the vorticity magnitude enables to determine with a good accuracy the trajectory of the trailing vortices [4]. Thus, the method based on the vorticity magnitude has been used in this work.

The software Fluent determines a vorticity magnitude. However, this vorticity magnitude is an absolute value and, so, does not enable to discriminate the two vortices generated above and below the disk. Indeed, the senses of rotation of the upper and lower ring vortices are of opposite sign.

In this study, the vorticity magnitude normal to the acquisition plane is defined from phase-averaged velocity gradients as follows [4,14]:

$$\omega = \frac{\partial \langle U_1^p \rangle}{\partial x_3} - \frac{\partial \langle U_3^p \rangle}{\partial x_1} \quad (1)$$

Where x_3 and x_1 represent respectively the axial and radial coordinates in the plane and p is the index of the blade position relative to the fixed acquisition plane.

This definition enables to readily discriminate the two vortices generated above and below the disk. The values of the vorticity of the upper and lower vortex are negative and positive respectively. Thus, the axis of the upper vortex corresponds to the minimum value of vorticity and the axis of the lower vortex to the maximum value. In Fig. 3 (RANS) and Fig. 4 (LES),

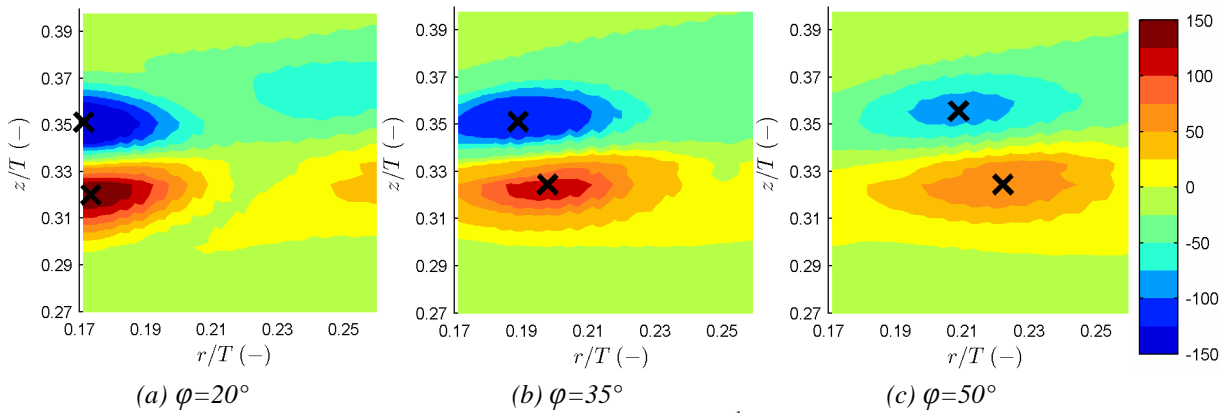


Fig. 3: RANS simulation - Phase-averaged vorticity magnitude (s^{-1}) for three positions of the blade relative to the acquisition plane.

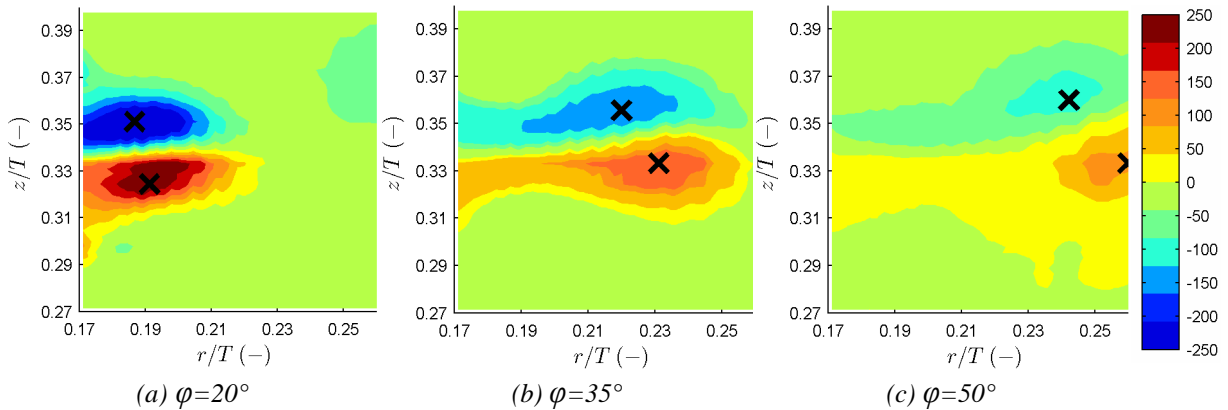


Fig. 4: LES simulation - Phase-averaged vorticity magnitude (s^{-1}) for three positions of the blade relative to the acquisition plane.

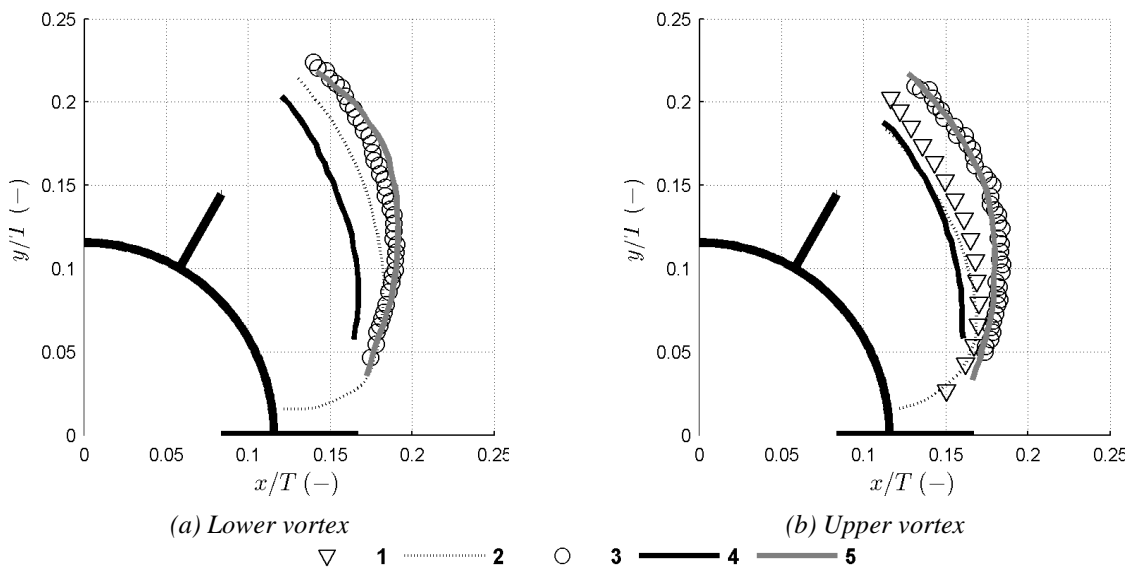
are presented the contours of vorticity magnitude on the acquisition plane for three positions of the blade $\varphi = 20, 35$ and 50° where φ represents the angle between the blade and the acquisition plane. On these figures, the cross corresponds to the maximum or minimum of vorticity magnitude and so to the axis of each vortex.

3.2 Trajectories of trailing vortices

For both RANS and LES simulations, the positions of the axis of the lower vortex and the upper vortex are plotted in Fig. 5. This numerical results are compared to the experimental works of Yianneskis et al. (1987) [7] and Escudié et al. (2004) [4] and to the numerical work (Large Eddy Simulation) of Derksen et al. (1999) [12]. In all the work cited, the configurations of the various stirred tanks are similar with concern to clearance ($C = T/3$), impeller diameter ($D = T/3$), blade width ($w = D/5$) and length ($l_b = D/4$). However, there is a difference in blade thickness (t_b): in the present configuration, also used by Escudié et al. [4] $t_b = 0.013D$, in Yianneskis et al. [7] $t_b = 0.03D$ and in Derksen et al. [12] $t_b = 0.017D$.

For RANS simulation, the axes of the two vortices are significantly closer to the impeller that determined in the experimental work carried out in the same tank. This can be attributed to the failure of RANS-based simulation to represent the periodic motion generated by the blade rotation. Because of the Reynolds decomposition, a RANS simulation does not take into account the shear stress induced by periodic velocities in the momentum equations. Thus, the periodic velocities are significantly underestimated near the blade tip.

The positions of the axis of the two trailing vortices calculated from LES results are in excellent agreement with the axis calculated from PIV measurements realized in the same vessel [4]. Unlike the RANS simulation, the LES simulation solves directly the velocities associated to the periodic motion (the grid size is smaller than the typical length of the trailing vortices). When compared to other studies, the difference can be attributed to the blade thickness that is known to have an influence on velocity field [16]. Moreover, in the numerical work from [12] the axis of each trailing vortex has been determined for a fixed axial coordinate. However, the axis of each trailing vortex is not located at a constant axial position: when the distance from the blade increases the axis of the vortices moves slightly upward (see Fig. 3 and Fig. 4 and the work of [4]), so that the location of the trailing vortices is found closer to the impeller in the work of [12].



1: from [7] (LDA), 2: from [12] (LES), 3: from [1] (PIV), 4: this work (RANS), 5: this work (LES)
 Fig. 5: Comparison of the locations of the axis of the (a) lower vortex and (b) upper vortex.

3.3 Relationship between trailing vortex location and turbulence

The core of a trailing vortex is associated with high levels of turbulent kinetic energy [4,9,12,14]. This is due to the transfer of energy between periodic motion and turbulence which is located in the trailing vortex core [1,4]. As a consequence, the maximum level of turbulence dissipation rate is likely to occur near the trailing vortices.

The contours of turbulent kinetic energy are plotted on Fig. 6 for RANS simulation and on Fig. 7 for LES. The trailing vortex cores are represented by a thick line corresponding to an isovalue of absolute vorticity $|\omega|$. For LES, the maximum value of turbulent kinetic energy is clearly located in the trailing vortex core. No clear relation between trailing vortex location and maximum level of turbulent kinetic energy is observed for RANS simulation. It should be pointed out that the turbulent kinetic energy calculated from LES results are in excellent agreement with PIV experiments from [3,4]. Although the RANS simulation predicts well the total kinetic energy, its repartition between periodic kinetic energy and turbulent kinetic energy is not correctly described: near the blade tip where the periodic kinetic energy should be high the simulation underestimates significantly the periodic kinetic energy and overestimates the turbulent one [1]. This can be related to the turbulent kinetic energy equation resolved by RANS simulation which does not take into account the energy transfer between periodic motion and turbulent motion. So, the energy of the mean motion is directly transferred to the turbulent one and the turbulent kinetic energy is maximum at the blade tip for RANS simulation.

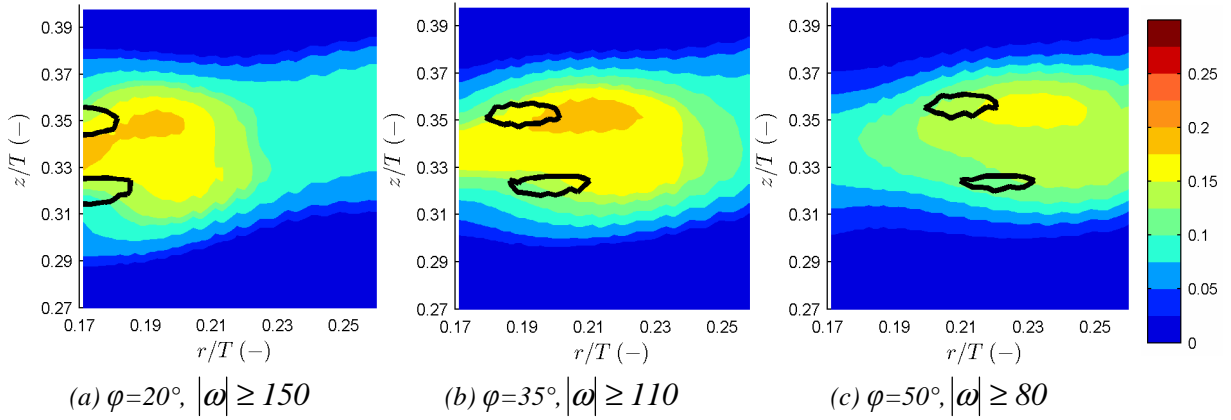


Fig. 6: RANS simulation - Phase-averaged turbulent kinetic energy ($m^2.s^{-2}$) for three positions of the blade relative to the acquisition plane.

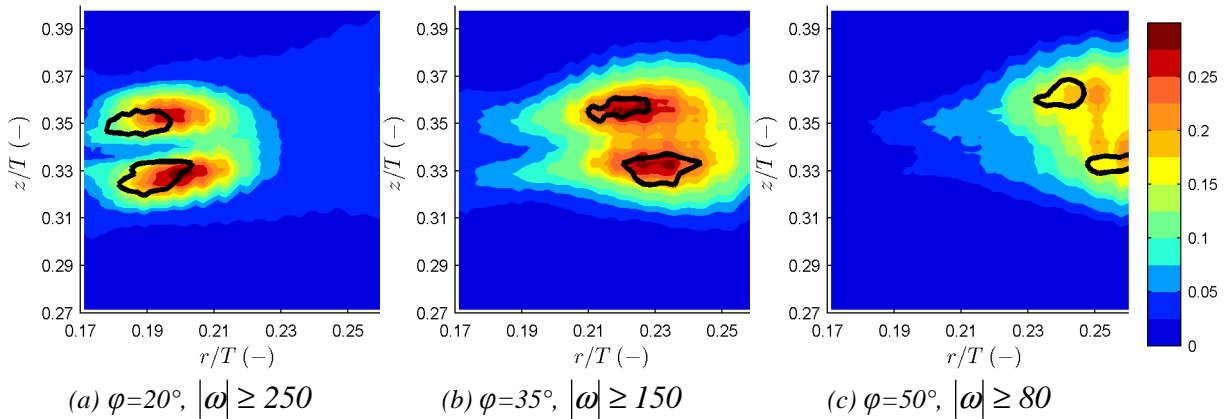


Fig. 7: LES simulation - Phase-averaged turbulent kinetic energy ($m^2.s^{-2}$) for three positions of the blade relative to the acquisition plane.

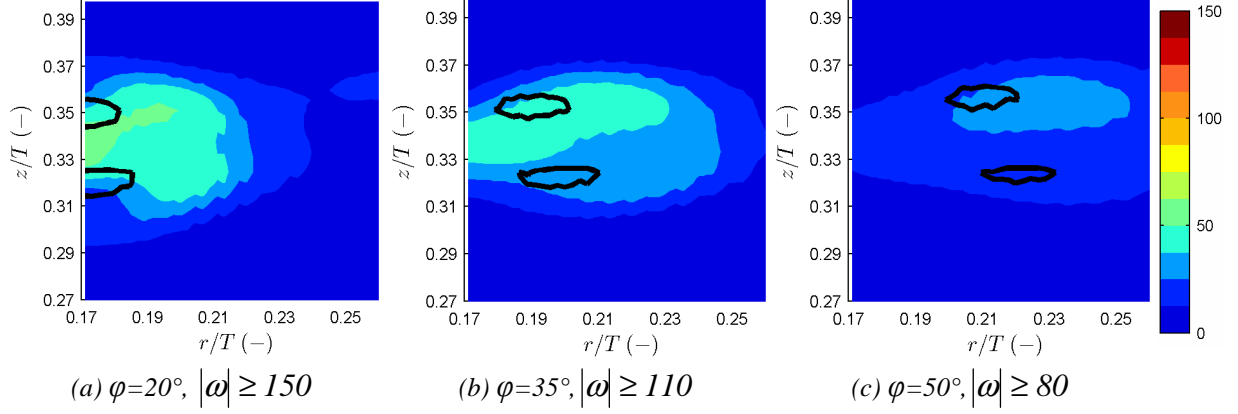


Fig. 8: RANS simulation - Phase-averaged turbulence dissipation rate ($m^2.s^{-3}$) for three positions of the blade relative to the acquisition plane.

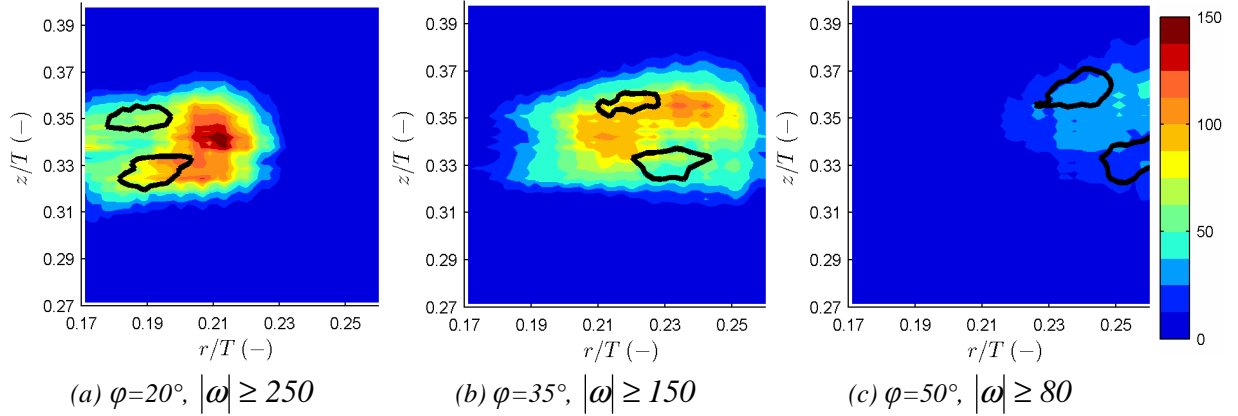


Fig. 9: LES simulation - Phase-averaged turbulence dissipation rate ($m^2.s^{-3}$) for three positions of the blade relative to the acquisition plane.

The contours of phase-averaged turbulence dissipation rate are plotted in Fig. 8 and Fig. 9 for RANS and LES simulations respectively. On these figures the local dissipation rate is normalized by the overall dissipation rate in the tank calculated for each simulation.

Although, the RANS simulation predicts the well amount of mean overall dissipation rate the evolution of the local dissipation rate in the impeller discharge is not well represented. It can be observed that the maximum values of the local dissipation rate correspond to the maximum values of turbulent kinetic energy determined by the RANS simulation.

From LES results, it may be noted that the maximum levels of dissipation rate are observed not directly in the core of the trailing vortices but in their vicinity. This is in good agreement with the results of Escudié et al. [3]. They have shown that the kinetic energy transfer between periodic and turbulent motions is an important term of the turbulent kinetic energy balance used for the calculation of the dissipation rate in their study. Moreover, when compared to various experimental works, the radial evolution of the time-averaged local dissipation calculated from LES results is well predicted (see Fig. 2 (a) and [1]).

4. CONCLUSION

In this article, we have investigated the ability of a RANS-based simulation and a Large Eddy Simulation to represent the trailing vortices generated behind the blades of a Rushton turbine.

Because the Reynolds-Averaged Navier-Stokes equations do not consider the periodic motion induced by the blade rotation, a RANS simulation is not able to reproduce the trajectory of the trailing vortices. Moreover, the turbulence properties, which are linked to the trailing vortices in the impeller discharge, are not well predicted.

On the contrary, the results obtained from LES are in excellent agreement with results obtained from PIV measurements realized in the same tank. The trajectory of each trailing vortex is well predicted and the results in term of turbulence properties show a strong correlation between turbulence and trailing vortices. The values of turbulent kinetic energy are maximum in the trailing vortex core. The turbulence dissipation rate in the impeller discharge is also linked to the position of the trailing vortices: the maximum levels are observed in the vicinity of the trailing vortices, where the energy transfer between periodic and turbulent motions takes place.

6. REFERENCES

1. Delafosse A., Liné A., Morchain J., Guiraud P., 2008. "LES and URANS simulations of hydrodynamics in mixing tank: Comparison to PIV experiments", *Chemical Engineering Research and Design* (publication in process).
2. Escudié R., 2001. "Structure locale de l'hydrodynamique générée par une turbine de Rushton", *Ph-D report*, n°628, INSA de Toulouse, France.
3. Escudié R., Liné A., 2003. "Experimental analysis of hydrodynamics in a radially agitated tank", *AIChE Journal*, **49**, 585-603.
4. Escudié R., Bouyer D., Liné A., 2004. "Characterization of trailing vortices generated by a Rushton turbine", *AIChE Journal*, **50**(1), 75-86.
5. Ducci A., Yianneskis M., 2005. "Direct determination of energy dissipation in stirred vessels with two-point LDA", *AIChE Journal*, **51**, 2133-2149.
6. Van't Riet K., Smith J.M., 1975. "The trailing vortex system produced by Rushton turbine agitators", *Chemical Engineering Science*, **30**, 1093-1105.
7. Yianneskis M., Popiolek Z., Withelaw J.H., 1987. "An experimental study of the steady and unsteady flow characteristics of stirred reactors", *Journal of Fluid Mechanics*, **175**, 537-555.
8. Stoots C.M., Calabrese R.V., 1995. "The mean velocity field relative to a Rushton turbine blade", *AIChE Journal*, **41**(1), 1-11.
9. Lee K.C., Yianneskis M., 1998. "Turbulence properties of the impeller stream of a Rushton turbine", *AIChE Journal*, **44**(1), 13-24.
10. Lu W.-M., Yang B.-S., 1998. "Effect of blade pitch on the structure of the trailing vortex around Rushton turbine impellers", *The Canadian Journal of Chemical Engineering*, **76**, 556-562.
11. Derksen J.J., Doelman M.S. Van Den Akker H.E.A, 1999. "Three-dimensional LDA measurements in the impeller region of a turbulently stirred tank", *Experiments in Fluids*, **27**, 522-532.
12. Derksen J.J, Van Den Akker H.E.A, 1999. "Large Eddy Simulations on the flow driven by a Rushton turbine", *AIChE Journal*, **45**(2), 209-221.
13. Schaefer M., Hofken M., Durst F., 2000. "Turbulence generation by different types of impellers", *Proceedings of the 10th European Conference on Mixing* (Delft, 2-5 July), Elsevier.
14. Sharp K.V., Adrian R.J., 2001. "PIV Study of Small-Scale Flow Structure around a Rushton Turbine", *AIChE Journal*, **47**(4), 766-778.
15. Jeong J., Hussain F., 1995. "On the identification of a vortex", *Journal of Fluid Mechanics*, **285**, 69-94.
16. Rutherford K., Lee K.C., Mahmoudi S.M.S, Yianneskis M., 1996. "The influence of Rushton impeller blade and disk thickness on the mixing characteristics of stirred vessels", *Trans. I.Chem.E.*, **74**, Part A, 369-378.